Chinese-Noodle-Inspired Muscle Myofiber Fabrication

*Yuhui Li, Chi Tat Poon, Moxiao Li, Tian Jian Lu, Belinda Pingguan-Murphy, and Feng Xu**

Much effort has been made to engineer artificial fiber-shaped cellular constructs that can be potentially used as muscle fibers or blood vessels. However, existing microfiber-based approaches for culturing cells are still limited to 2D systems, compatible with a restricted number of polymers (e.g., alginate) and always lacking in situ mechanical stimulation. Here, a simple, facile, and high-throughput technique is reported to fabricate 3D cell-laden hydrogel microfibers (named hydrogel noodles), inspired by the fabrication approach for Chinese Hele noodle. A magnetically actuated and noncontact method to apply tensile stretch on hydrogel noodles has also been developed. With this method, it is found that cellular strain-threshold and saturation behaviors in hydrogel noodles differ substantially from their 2D analogs, including proliferation, spreading, and alignment. Moreover, it is shown that these cell-laden microfibers can induce muscle myofiber formation by tensile stretching alone. This easily adaptable platform holds great potential for the creation of functional tissue constructs and probing mechanobiology in three dimensions.

1. Introduction

Tissues within human body are mostly formed with specific structures to enable designated functions. Fiber-shaped structures are one of the most commonly found tissue components in vivo, which are mostly microscale and play an important role in maintaining tissue functionality.[1,2] One typical example is the striated muscle fiber in cardiac and skeletal muscles.[3] Such fiber-shaped tissue structures can actively generate sufficient contractile forces for a variety of physiological movements, such as heart beating and muscle contraction.[4,5] Other examples are blood vessels and neural pathways (e.g., continuous fibrous structure of cerebral pathways).[2,6,7] Much effort has been made to engineer cell-derived constructs based on 2D systems. However, maintaining specific functionality over longer periods of time has proved difficult, and they lack the architecture of native tissues, which are always in 3D microenvironments.[8–11] Therefore, it is necessary to develop in vitro 3D culture models for fabricating fiber-shaped cell-derived constructs with specific architecture and functionality for tissue assembly and remodeling applications.

To implement a 3D fiber-based strategy, cell-laden hydrogel microfibers have been investigated due to their water-swollen, highly physically, and chemically tunable properties mimicking native extracellular matrixes (ECMs). Such microfibers are commonly fabricated through well-developed approaches, including microfluidic spinning,[12–14] electrospinning,[15] wetspinning,[16,17] and interfacial complexation.[18] A number of cell types (endothelial cell, fibroblast, cortical cell, and cardiomyocyte) have been used to generate 3D tissue constructs that mimic blood vessels, nerve networks, and cardiac fibers.[6] In these systems, external stimulations are commonly applied for enhancing functions of engineered tissue constructs. For instance, growth of blood vessels in vivo experienced naturally mechanical stresses (e.g., shear or tensile stress), which play an important role in influencing tissue mechanical properties and permeability.[19–22] Mechanical stretching during tissue culture has been found to improve the properties of tissue-engineered blood vessel constructs (cell-laden collagen hydrogel) in terms of mechanical strength and histological organization.[23] In these systems, a major challenge is the temporary and unstable mechanical loading process caused by the mechanical weakness of such hydrogels. Other fabrication strategies to generate functional tissue constructs include microfluidic spinning,[12–14] electrospinning,[15] wetspinning,[16,17] and interfacial complexation.[18] Although such techniques overcome the problem of generating fibers with topographical architecture, it is still limited by the restricted number of biomaterials (e.g., calcium alginate[24] and supramolecular hydrogels),[25,26] which lack bioactivity for cell growth.[27] A variety of studies have proposed to enhance cell adhesion on alginate fibers by covalently linking peptide sequences (e.g., Arg-Gly-Asp, RGD and Val-Ala-Pro-Gly, VAPG). However, peptides are expensive and the modification

Y. Li, Prof. F. Xu
The Key Laboratory of Biomedical Information Engineering of Ministry of Education
School of Life Science and Technology
Xi'an Jiaotong University
Xi'an 710049, China
E-mail: fengxu@mail.xjtu.edu.cn
Y. Li, C. T. Poon, M. Li, Prof. T. J. Lu, Prof. F. Xu
Bioinspired Engineering and Biomechanics Center
Xi'an Jiaotong University
Xi'an 710049, China
C. T. Poon, Prof. B. Pingguan-Murphy
Department of Biomedical Engineering
Faculty of Engineering
University of Malaya
Kuala Lumpur 50603, Malaysia

DOI: 10.1002/adfm.201502018

process is complex and time consuming.[28,29] Moreover, these studies usually fabricate cell-laden microfibers by embedding dispersed cells within hydrogel precursor followed by a chemical crosslinking reaction. The cell-laden hydrogel precursor is easily exposed to chemicals, high voltages, and/or high temperatures during gelation, which may involve the issues of damage to the sensitive biological materials (e.g., cells) loaded in the fiber, and loss of their function.[8] Additionally, the aforementioned approaches require a rather complex setup and need the assistance of specialist equipment to generate the fibers, which is often costly and thus inaccessible to many settings. Therefore, there is a necessary and urgent need for a simple, facile, and low-cost method for fabrication of cell-laden microfiber which is not harmful to cells.

Further, in vivo tissues are always under mechanical stimulation, which in itself is important for the induction of both normal and pathological tissues formation.[30,31] For instance, skeletal muscle tissue is exposed to a tensile strain of <4% under physiological conditions, and to strain of 8%–10% under pathological conditions (e.g., rupture).[32] Cellular responses to mechanical cues are crucial in tissue remodeling, healing, and homeostasis, while dysregulation of these responses is believed to underlie many important diseases, such as metastatic cancer.[33,34] Existing methods build upon the large set of tools for probing mechanobiology in 2D, such as micropost arrays,[35] stretchable substrata,[36] and 2D traction microscopy.[37] However, cells normally reside in a 3D environment embedded in an ECM and behave very differently when cultured in 2D,[38,39] such as their expression of key mechanical proteins associated with adhesion to ECM.[40] Thus, defining the mechanical responses of cells embedded in 3D ECM is a pressing need. A number of systems have been developed to apply mechanical loading on cell-laden 3D hydrogel matrix, including ring-like tissue constructs,[41] and tissue constructs adhered to flexible substrates.[42] However, important challenges that these systems face include obtaining statistically significant sample size, heterogeneous deformation, and complexity of the system setup process. Additionally, manipulation and mechanical loading process of cell-laden ECM is temporary and unstable due to the mechanical weakness of hydrogels. Therefore, it is necessary to develop a noncontact mechanical loading method for engineering functionally enhanced tissues.

Here, we describe a simple, facile and high-throughput method to prepare cell-laden hydrogel microfiber-based constructs, named hydrogel noodles, inspired by the fabrication approach for Chinese Hele noodle, a famous Chinese traditional food formed by pressing the dough mixture through a sieve (Movie S1, Supporting Information). Gelatin methacrylate (GelMA), a biocompatible and photocrosslinkable hydrogel derived from natural gelatin that is effective for 3D cell encapsulation,[43,44] and poly(ethylene glycol) dimethacrylate (PEGDMA), with relatively high hydrogel mechanical properties,[45] were both used here to fabricate hydrogel noodles. Hundreds to thousands of hydrogel noodles can be created within a few seconds. We then developed a magnetically actuated and noncontact method to apply tensile stretch on such fabricated hydrogel noodles. A key enabling feature of these experiments was the simplicity of the noodle fabrication process. The high-throughput character reduced challenges associated with specimen-to-specimen variability. The noncontact loading afforded by the focused magnetic fields enabled uniformity of the loading environment, simplifying interpretation of the results. Additionally, the fabrication process does not affect cell biological functions and is compatible with various cell types. This platform overcomes challenges faced by other 3D culture systems associated with sample handling and diffusion barriers of mechanical loading. This method also enabled the first ever generation of C2C12 muscle myofibers in hydrogel noodles under only tensile stretching, as characterized in terms of proteins and gene expression related to muscle myoblast differentiation. Such fabrication and mechanical loading strategy provides an easily adaptable platform to create functional tissue constructs and tools for probing mechanobiology in 3D.

2. Results and Discussion

2.1. Fabrication and Characterization of Hydrogel Noodles

We fabricated hydrogel noodles using a simple photolithography strategy. Two kinds of hydrogels have been used here, GelMA and PEGDMA. We have previously demonstrated that GelMA hydrogels emulated the ECM for multiple cell types, such as that of muscle, neuron, cardiac, and endothelial cells.[46,47] The PEGDMA photodegradable hydrogels was used to enhance the mechanical properties of fabricated hydrogel noodles. Briefly, GelMA and PEGDMA were dissolved in distilled water before adding photo-crosslink initiator (2-hydoxy-2-methylpropiophenone). Three mass ratios of PEGDMA/GelMA (W_p:W_g) at 2:1, 3:1, and 4:1 were mixed in distilled water. The prepolymer solution was filled in a syringe without adaptor part and exposed to 365 nm UV light for crosslinking purposes. The crosslinked hydrogel within the syringe was then squeezed through scientific sieves (**Figure 1**a and Movie S2, Supporting Information). To evaluate the influence of sieve hole size on the morphology of ultimately fabricated hydrogel noodles, we used two kinds of sieves, sieve-100 with pore size of 129 ± 11 μm and sieve-40 with pore size of 322 ± 7 μm (Figure 1b and Figure S1, Supporting Information). Homogeneous diameter, shape, and length of fabricated hydrogel noodles were observed (Figure S2, Supporting Information). The morphology of hydrogel noodles was also similar regardless of varying PEGDMA/GelMA mass ratio (Figure 1c and Figure S2, Supporting Information). These results demonstrate that noodle-shaped hydrogels can be fabricated using a simple and low-cost sieve within a few seconds. To study the effect of the photocrosslinking process on the morphology of the hydrogel noodle, we fabricated noodles using different UV crosslinking times (15, 30, 45, and 60 s). We found that the noodles prepared from 2:1 hardly crosslinked (or did not crosslink completely) unless exposed to UV at 365 nm for at least 45 s, and hence hydrogel noodle could not be fabricated under such a crosslinking condition as a result of the low polymer and photocrosslink initiator fraction in the prepolymer solution. There is no significant difference between the largest and smallest diameter of the fabricated noodle (Sieve-100: largest diameter = 130 ± 16 μm (W_p:W_g, 3:1, UV, 30 s), smallest diameter = 117 ± 15 μm (W_p:W_g, 4:1, UV, 45 s), p = 0.245. Sieve-40:

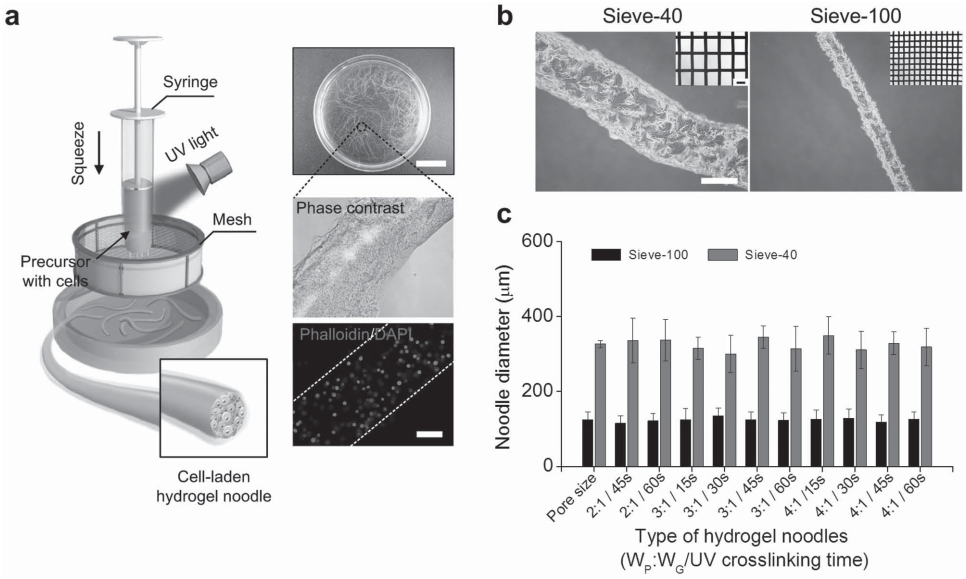

Figure 1. Fabrication of hydrogel noodles. a) Schematic representation of the fabrication process for fiber-shaped hydrogel noodles. The prepolymer solution was filled in a syringe without adaptor part and exposed to 365 nm UV light for photocrosslinking. Thousands of hydrogel noodles were fabricated within seconds by squeezing the hydrogel through a scientific sieve. Phase contrast and fluorescent images showed the cell populations encapsulated in hydrogel noodles. b) Bright-field microscopic images of fabricated noodles (2:1/45 s) and pore structure of sieves with different size, sieve-40 for (left) and sieve-100 for (right). c) The effect of crosslinking process on the morphology of hydrogel noodles. The diameter of hydrogel noodles was similar regardless of varying sieve pore size, PEGDMA/GelMA mass ratio, and UV crosslinking time. Error bars, SD ($n = 10$). Scale bars: a) 1 cm (top), 100 μm (bottom), b) 250 μm.

largest diameter = 333 ± 38 μm (W_p:W_g, 4:1, UV, 15 s), smallest diameter = 292 ± 48 μm (W_p:W_g, 3:1, UV, 30 s), $p = 0.315$) at significant level of $p < 0.05$. These results indicate that the determinant of the diameter of noodle is the pore size of sieve, instead of hydrogel fabrication parameters. The deviation of noodle diameter from pore size of sieve is in the range of tens of micrometers.

2.2. Magnetically Actuated Loading Method Inspired by Stretching Process of Chinese Noodles

To apply mechanical stimulus on cell-laden hydrogel noodles, we developed a magnetic-assisted loading method, which can undergo reversible, relatively homogeneous strain up to 10% following noncontact magnetic actuation. Briefly, cell-laden hydrogel noodle each contained one stiff, strong "magnetically actuated" layer of PEGDMA (20% w/v) encapsulating iron microspheres with uniform size, following photo-crosslinking process (**Figure 2**a,b), which was used for uniaxial stretching. The displacement of another layer was constrained to be zero by encapsulating more microspheres (>10) inside. The hysteresis loop has shown good magnetic responsive properties of iron microsphere, and thereby can be subsequently utilized for actuating hydrogel noodles by inducing tensile strain (Figure 2c). The interface between the two layers was toughened using the double-network method.[48] To avoid differential swelling of the "magnetically actuated" layer and the hydrogel noodle itself, we measured the swelling ratio of two kinds of hydrogels and found that the swelling ratio of the PEGDMA layer was relatively constant over the concentration range of 15%–20% (w/v). This could be matched by tuning the mass ratios of PEGDMA/GelMA noodles (Figure S3, Supporting Information). To stretch cell-laden hydrogel noodles, the encapsulated ion microspheres were actuated using a NdFeB magnet (45 mm in length, 10 mm in width, and 5 mm in thickness) (Figure 2d). Both simulation and experimental results show that the maximum magnetic field strength in the *y*-axis can be obtained by decreasing the separation between the "magnetically actuated" layer and the end surface of permanent magnet (Figure 2e,f). Such noncontact magnetic actuation can easily apply mechanical stimulus to cells encapsulated in hybrid hydrogels with weak mechanical properties, avoid perturbations introduced by sample handling, and even test the mechanical contributions of cells and their secreted ECMs.

2.3. Mechanical Characterization of Hydrogel Noodles

To characterize the mechanical properties of fabricated hydrogel noodles, we measured their elastic modulus by calculating the magnetic force applied to the ion microsphere and measuring the axial deformation of hydrogel noodles under uniaxial stretching, respectively. We first simulated the magnetic force by predicting the magnetic field gradients experienced by the iron microspheres using finite element simulation (Figure 2g and Figure S4, Supporting Information). To experimentally measure magnetic force applied to iron microspheres in "magnetically actuated" layers, the Stokes drag method was used.[49] Both the simulation and experimental results show that the relationship between force and separation was nearly inverse cubic (Figure 2g). The tensile stress

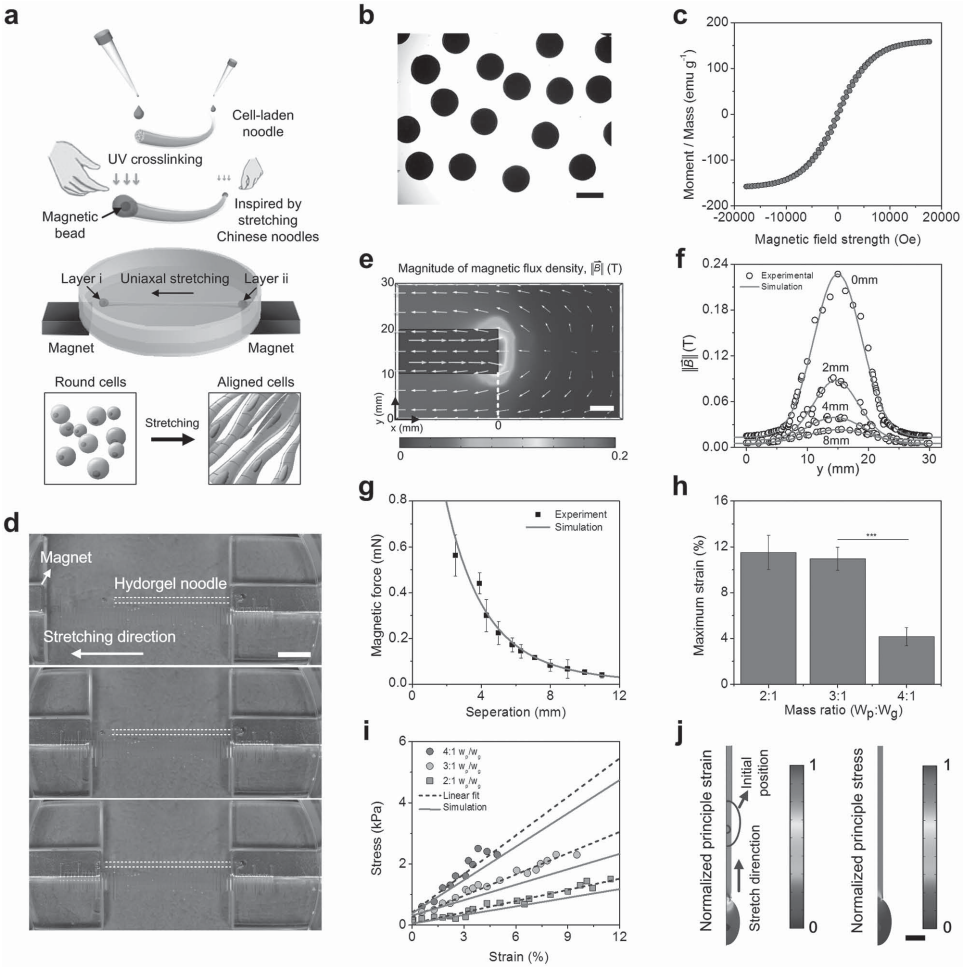

Figure 2. Magnetically actuated loading method to stretch hydrogel noodles. a) Schematic of noncontact and magnetically actuated loading method, inspired by stretching fabrication of Chinese Hele noodles. Each magnetically actuated hydrogel noodle contains two layers: i) "magnetically actuated" layer encapsulated with one iron microsphere; ii) constrained layer encapsulated with >10 microspheres. Permanent magnet was controlled by a linear stage. Straining can significantly enhance cell alignment in hydrogel noodles. b) Microscopic image of iron microspheres in a uniform size. c) Specific magnetization of a single iron microsphere. Magnetic moment per unit mass showed very little hysteresis. From these measurements, the saturation moment was estimated as $M_{sat} = 152$ emu g^{-1}. d) Images of stretched hydrogel noodle in varying strain. Permanent magnet moved close to the "magnetically actuated" layer of hydrogel noodle from left side. e,f) Finite element simulation of magnetic field distribution around the free end of magnet. Shown are a contour plot and graph of the magnitude of the magnetic flux density. Data plots in (f) represent the experimental results of magnetic flux density distributed in the *y*-axis using a Teslameter. g) The magnetic force was an approximately inverse-cubic function of the separation between the end of magnet and the iron microsphere. h) We maximized the failure strain that hydrogel noodles could withstand prior to failure by modulating the PEGDMA/GelMA fraction. i) Representative stress–strain curves for hydrogel noodles composed of different PEGDMA/GelMA fraction were highly linear. j) Simulated strain (left) and stress (right) distributions in hydrogel noodles under magnetic actuation showed highly uniform mechanical fields. Contours were normalized to the peak values. Error bars, SD ($n = 10$, $^{***}p < 0.001$). Scale bars: b) 200 μm, d) 5 mm, e) 2 mm, j) 500 μm.

of hydrogel noodles was calculated using $\sigma = F_{magnetic}/A$, where A is the cross-sectional area. To further investigate the effect of PEGDMA/GelMA mass ratio on tensile strain of hydrogel noodles, we stretched noodles made from mass ratio (W_p:W_g) at 2:1, 3:1, 4:1 and analyzed the deformation of stretched noodles from microscopy images. The maximum strain levels of tested noodles were 11.62 ± 1.51%, 10.95 ± 1.04%, and 4.22 ± 0.86%, indicating that hydrogel noodle becomes significantly stiffer beyond a threshold of PEGDMA/GelMA mass ratio (Figure 2h). The resulting stress/strain curves of hydrogel noodles (embedded with 6×10^3 cells for each sample) were nearly linear and noodle elastic modulus was 12.19 ± 1.6 kPa, 23.16 ± 0.8 kPa, and 42.05 ± 1.5 kPa for mass ratio 2:1, 3:1, and 4:1, respectively (the slope of these curves, $E = d\sigma/d\varepsilon$; Figure 2i). To clarify the cell and matrix contribution to the hydrogel noodles' mechanical properties, noodle samples (under 10% strain) with different embedded cell numbers were culturing for 3 d and then utilized for mechanical test (Figure S5, Supporting Information). The results suggested that mechanical properties of single hydrogel noodle can be enhanced by increasing the embedded cell number up to 6×10^5, which is possibly caused by the proliferated cell populations and their secreted ECMs (e.g., collagen). Further studies focused on ECM remodeling and metabolism under mechanical loading are needed. To analyze the stress/strain distribution on stretched hydrogel noodles, we simulated the stress applied to the hydrogel noodle,

assuming PEGDMA/GelMA (W_p:W_g/2:1) as an incompressible, isotopic Neo-Hookean solid with elastic modulus derived from experimental work described below (Figure 2j). Finite element simulation results indicated that the strain fields within the hydrogel noodle were uniform to within a few percent except close to free edges of the interface between the "magnetically actuated" layer and PEGDMA/GelMA layer. Since there is still some deviation between the strains on hydrogel and on cells due to the slippery boundary between hydrogel and cells, the exact tensile strain exerted on each of the embedded cells is still unclear. Up to date, particle-tracking methods have been developed to quantitatively measure cell tractions in a 3D hydrogel matrix.[50,51] In these systems, a number of fluorescent microparticles were also encapsulated in hydrogels for obtaining strain map. Cells in 3D hydrogels deformed the surrounding matrix, which was visualized by tracking the displacements of encapsulated fluorescent microparticles in the vicinity of each cell. However, there is still lack of studies focusing on the relationship between applied strain on hydrogel and single cells. These particle-tracking methods can be selected as prior candidate for addressing this challenge.

2.4. Uniaxial Stretch Increases Cell Spreading and Proliferation in Hydrogel Noodles

To investigate the cell responses to uniaxial stretch in 3D, we first encapsulated C2C12 myoblasts in hydrogel noodles with a PEGDMA/GelMA fraction of 2:1, due to the larger strain range than groups at 3:1 and 4:1. The applied magnetic fields showed no statistically significant effects on cell responses independent of the mechanical stretches they actuated (Figure S6, Supporting Information). To distinguish the effect of stiffness and strain on cell behaviors, we tested cell responses under 10% strain levels considering the linear stress/strain relationship in this strain range (i.e., constant stiffness). We firstly tested the effect of hydrogel fabrication parameters, including shear stress induced by squeezing process, UV light density, and crosslinking time, on cell viability (Figure S7, Supporting Information). Live/dead staining results suggested that squeezing process did not affect cell viability, which is only declined by increasing the UV light density and crosslinking time. For unstretched hydrogel noodles, the encapsulated C2C12 myoblasts maintained a high cell viability (92.5% ± 1.5%) even after culture for 5 d, indicating that such PEGDMA/GelMA composites are biocompatible (**Figure 3**a,b). We also characterized the pore structure of hydrogel noodles with a PEGDMA/GelMA fraction of 2:1 (Figure S8, Supporting Information). Scanning electron microscopy (SEM) images indicated that the hydrogel noodle is composed of interconnected pore structure, high porosity, and uniform pore size, which was crucial for nutrient diffusion in hydrogel networks and maintain high cell viability. To avoid the effect of initial cell density on cell behaviors under different strain levels, the initial cell loading density of each strained group is kept the same of 1×10^6 cells per milliliter, i.e., $\approx 6 \times 10^3$cells for each noodle sample. We observed that cells in unstretched noodles (control group) kept a round shape even after 3 d of culturing, and shown limited ability to proliferate. This may be caused by the utilized stiff hydrogel noodles.[43] Surprisingly, cell spreading area and proliferation significantly increased under uniaxial stretching (>5% strain) after 3 d of culturing (Figure 3c). The same increasing trend of cell numbers in strained hydrogel noodles has also been demonstrated using nuclear staining (Figures S9 and S10, Supporting Information). Confocal fluorescent images of cell nucleus in strained hydrogel noodles have been taken at days 1, 3, 5, and 7, respectively. Quantification results indicated that 10% strain of noodles can significantly enhance the cell proliferation and increase to a saturation level after 5 d culturing. This difference may be caused by passive stretching of cells, and the lower spreading area in unstrained hydrogel noodles would not be expected if passive strain simply opened more volume for cells to occupy. Moreover, cell spreading area increased nonlinearly with increasing strain, rising rapidly to an asymptotic saturation level at a critical stretching time in the range of 70 h. Cell populations in hydrogel noodles also increased with increasing strain and the ≈7 d time interval that cell populations required to spread to steady-state mean size did not depend upon strain.

2.5. Uniaxial Stretch Induces Myofiber Generation in Hydrogel Noodles

Expansion of C2C12 myoblasts and formation of myotubes have been well achieved in 2D systems, through various platforms including micropatterned substrates,[52] aligned fibrous scaffolds,[53] and cell printing.[54] As demonstrated in these works, topological features have a great impact on alignment of C2C12 myoblasts in 2D, which is important for myofiber fabrication. In this process, myoblasts firstly align and fuse together in an end-to-end direction to form myotubes, which is crucial to maximize contractility and force generation within muscle tissues.[55] However, the large set of tools for creating such functional structures does not extend easily to 3D. In our systems, cell alignment in 3D hydrogel matrix (PEGDMA/GelMA fraction 2:1) induced by uniaxial stretching (10% strain), for the first time, was observed. Cells in unstrained hydrogel noodles showed random orientation after encapsulation (embedded with 6×10^3 cells for each sample) (**Figure 4**a). However, cells in hydrogel noodles stretched at 10% for 7 d polarized perpendicular to the stretch direction and showed increasing polarization parallel to the stretch direction after 14 d stretching (Figure 4a). This observation indicated that cell alignment in a 3D matrix was a strong function of uniaxial stretching time, inconsistent with observations from 2D culture. Cells cultured on stretchable 2D substrate always tend to align perpendicular to the direction of principal strain (i.e., the direction of minimal substrate deformation), which is generally known as stretch-avoidance or strain-avoidance.[4] Next, differentiation of C2C12 myoblasts in stretched noodles was verified by fluorescent staining and protein content analysis of myosin heavy chain (MyHC) after stretching for 14 d (Figure 4b) as a standard measurement of myotube formation.[56] Here, C2C12 myoblasts were cultured on a 2D petri dish with specific culture medium composed of horse serum, which can induce myotube differentiation, as control. To clarity whether the myoblast differentiation is induced by tensile strain, we did control experiment by culturing cells

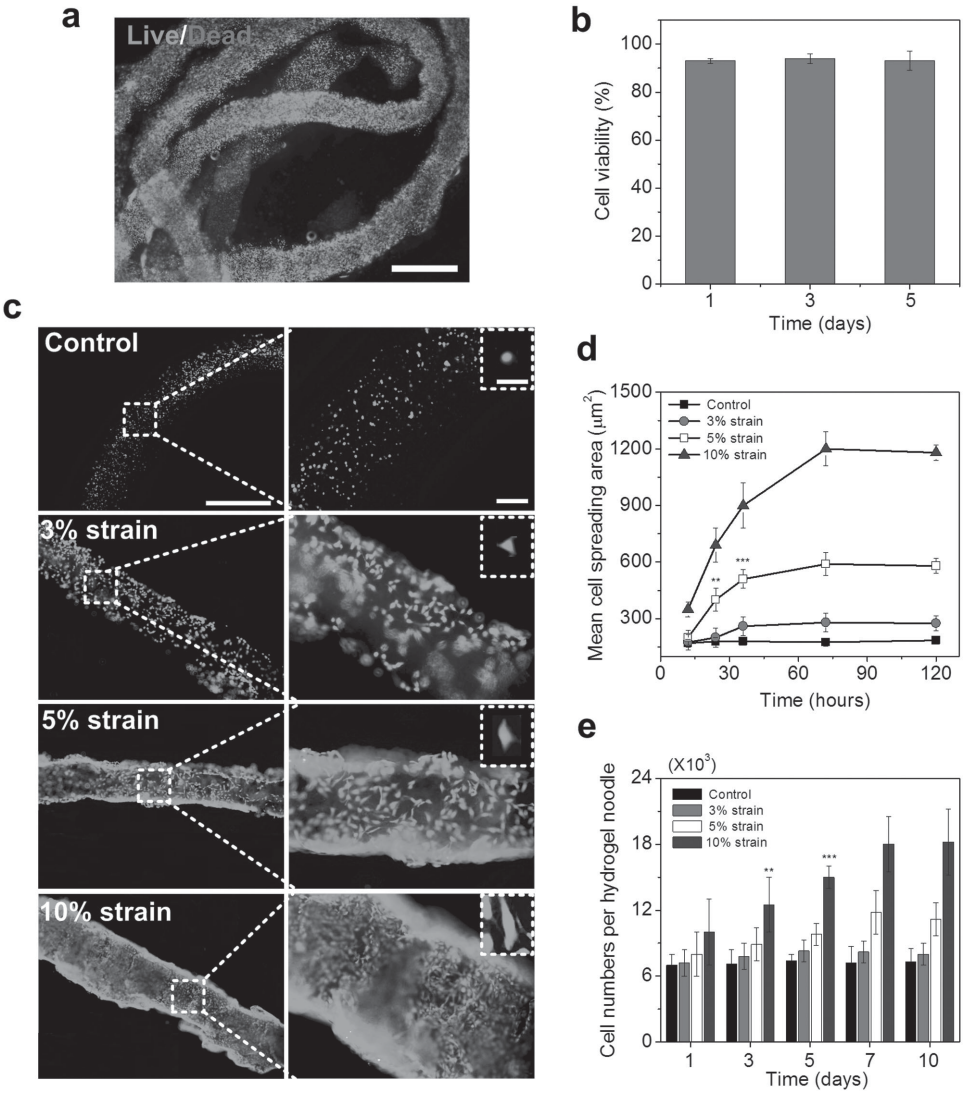

Figure 3. Viability, proliferation, and spread of C2C12 myoblasts within strained hydrogel noodles. a) Live/dead fluorescent images of cells in unstrained hydrogel noodles after 5 d. b) Quantitative analysis of live/dead fluorescent images showed overwhelmingly live (green) cells (>90%) and few dead (red) cells. c) Live/dead fluorescent images of cells in hydrogel noodles after 3 d of straining to different levels. d,e) Mean cell spreading area and cell numbers per hydrogel noodle increased with culture time and different strain levels, up to a threshold. Cell spreading area and proliferation can be significantly increased after uniaxial stretching (>5% strain) for 3 d. Error bars, SD ($n = 10$, $^{**}p < 0.01$, $^{***}p < 0.001$). Scale bars: a) 500 μm, c) 500 μm (left), 100 μm (right), and 50 μm (right in the box).

in strained and unstrained (Figure 4b) hydrogel noodles within Dulbecco's modified Eagle's medium (DMEM) without horse serum, which is known for its ability to induce myoblast differentiation. From our observations, cells in unstrained hydrogel noodles showed no spreading and proliferation responses to magnetic fields after 1, 3, or 5 d of culture. On the contrary, cells in strained groups showed significant alignment parallel to the stretch direction and myosin heavy chain formation after 14 d culturing, which revealed that there is strain dependence of cell alignment and further induces myoblast differentiation in a 3D matrix. With culture time, structural maturation of cell-derived hybrid noodles was evident from the progressive increase in myotube diameter (11.5 ± 1.2 μm and 25.8 ± 4.8 μm at 7 and 20 d of culture) (Figure 4c) and expression of skeleton muscle-specific protein MyHC (Figure 4d,e). In addition, the mRNA expression levels of the MyHC isoform (MyHC IId/x) were also significantly increased at day 14 of culture. Known transcriptional regulators of MyHC, mRNA levels of myogenic differentiation 1 (Myod), Myogenin, and Mrf4 were also found to be increased (Figure 4f–i). Most importantly, these results indicated that uniaxial stretching substantially promotes C2C12 myoblast differentiation and myofiber formation in 3D hydrogel noodles without the need of horse serum. Existing approaches for muscle myofiber fabrication are achieved by enhancing topographical microstructure and electrical conductivity of biomaterials.[57,58] However, in vivo tissues are always under mechanical stimulus, which is crucial for maintaining their structures and functions. Herein, we were able for the first time to successfully generate cell alignment in strained 3D hydrogel matrix, which is well known to exert significant effects

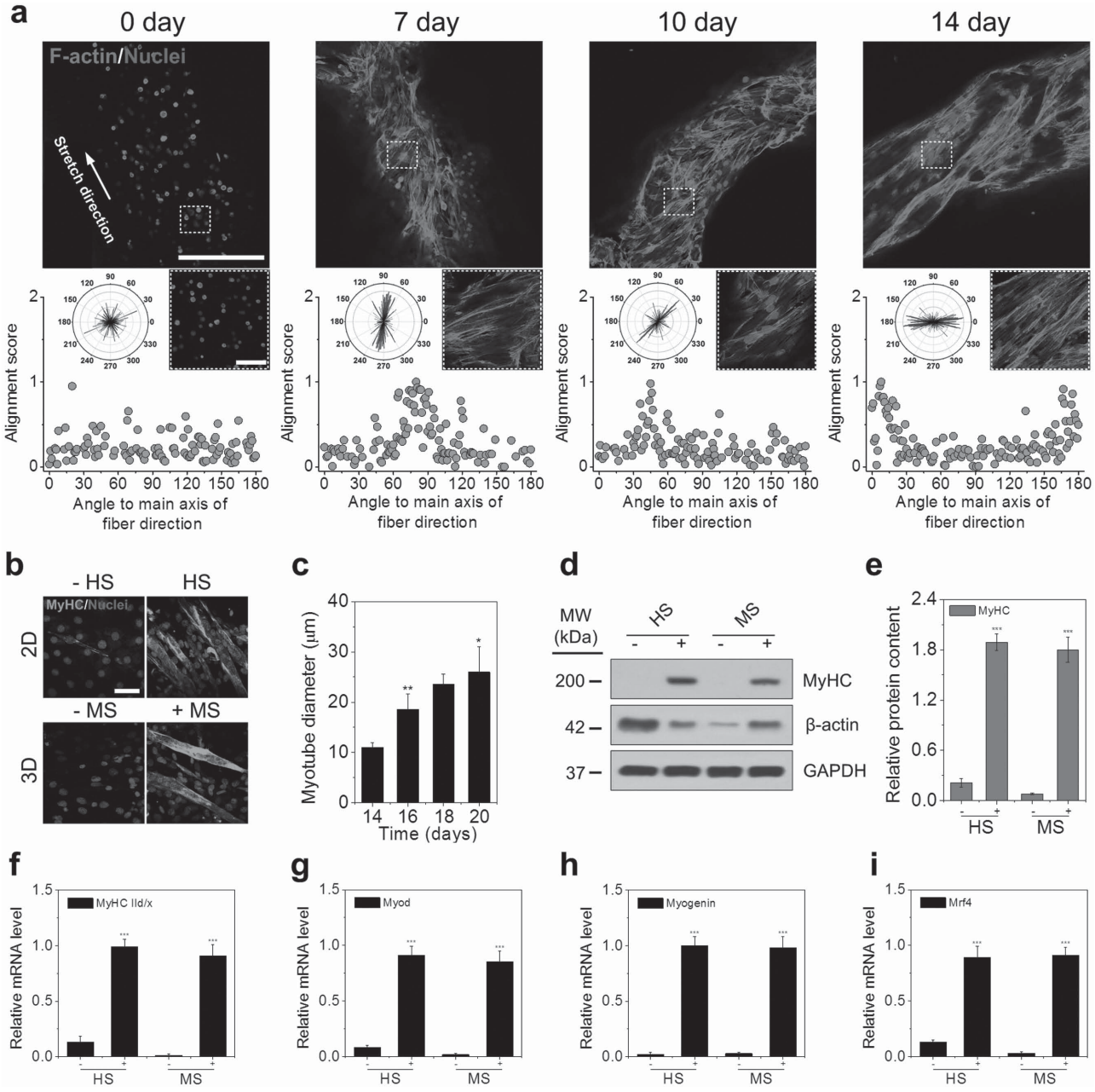

Figure 4. Alignment and differentiation of C2C12 myoblasts within strained hydrogel noodles. a) Confocal fluorescent images of C2C12 myoblasts in strained hydrogel noodles (red: F-actin (phalloidin); blue: nuclei (DAPI)). Cells in hydrogel noodles stretched 10% for 7 d polarized perpendicular to the stretch direction and showed increasing polarization parallel to the stretch direction after 14 d stretching. b) Confocal fluorescent images of myoblasts seeded on cover glass discs in six-well plates, with (+) and without (–) horse serum (HS) and in hydrogel noodles, with (+) and without (–) mechanical stimulation (MS) noodles at day 14 of culture. c) Myofiber diameter increases with time in culture, with significant enhancement at days 16 and 20 versus day 14 of culture. d,e) Western blot analysis of MyHC was used to confirm the efficiency of C2C12 myoblast differentiation. f–i) The mRNA contents of the MyHC isoform f) MyHC IId/x and MyHC regulators g) Myod, h) Myogenin, i) Mrf4 were analyzed by real-time PCR. Error bars, SD ($n = 10$, $*p < 0.05$, $**p < 0.01$, $***p < 0.001$). Scale bars: a) 300 μm (up), 50 μm (bottom), b) 50 μm.

on tissue regeneration and modulate mechanical properties of tissues including skeleton, cardiac muscle, and tendon.[4] Cells cultured on a 2D substrate that is subjected to uniaxial cyclic stretch trend to align perpendicular to the direction of principal cyclic strain (i.e., the direction of minimal substrate deformation), which is generally known as strain-avoidance. In contrast, in our observations orientation of cells cultured in 3D hydrogels turns out to align parallel to stretch direction. This is possibly because it is more difficult to alternate stress-fiber orientation in 3D constructs compared to 2D by stretching, which dominates cell alignment directionality.[4] It is postulated that other factors such as the contact guidance of the ECM fibers in the hydrogel will also impact stretch-induced alignment over time. We subsequently probe the effect of mechanical tensile

strain on myofiber generation in a simple 3D system, which holds potential to create functional tissue constructs and helps understand the mechanobiological responses of cells in 3D.

3. Conclusion

The developed approach allows for fabricating fiber-shaped hydrogel noodles in a spatially defined and high-throughput manner, obtaining thousands of samples within a few seconds. The fabrication process is simple and is not limited to the photolithography process and could also be extended to other kinds of crosslinking reactions (e.g., chemical and thermal). In addition, the high-throughput character reduces challenges associated with specimen-to-specimen variability. The noncontact loading afforded by external magnetic fields enables uniformity of the loading environment, controlling strain states and simplifying interpretation of the results. Herein, our systems have been successfully applied to engineer 3D myofibers with specific architecture and function, which holds great potential for creating functionally enhanced tissues and probing mechanobiology in 3D. We believe that hydrogel noodles provide useful and well-calibrated information about cellular response to mechanical stimulus that can be applied to future work in more complicated fibrous mechanical environments.

4. Experimental Section

Preparation of GelMA and Hydrogel Noodles: GelMA, a biocompatible and photocrosslinkable hydrogel that is effective for 3D cell encapsulation, was synthesized as described previously.[43] Briefly, type A porcine skin gelatin powder (Sigma-Aldrich) was added into Dulbecco's phosphate buffered saline (DPBS; Gibco BRL Life Technologies, Inc.) at a concentration of 10% (w/v) at a temperature of 65 °C, and stirred until fully dissolved. Methacrylate (Sigma-Aldrich) was added into this solution at a rate of 0.5 mL min^{-1} and stirred at 50 °C until the target volume was reached. The solution was then allowed to react for 3 h. The fraction of lysine groups that reacted could be controlled by varying the amount of added methacrylate. Following a five times dilution with additional warm (40 °C) DPBS to stop the reaction, the mixture was dialyzed against distilled water using 12–14 kDa cutoff dialysis tubing (Spectrum Labs, Inc.) at 40 °C for 2 weeks. Water was changed every day to remove salts and methacrylic acid. After that, the GelMA solution was lyophilized for 1 week to generate a porous foam and stored at −80 °C for further use.

GelMA and PEGDMA (MW = 1000, Polysciences, Inc.) were then dissolved in distilled water before added with 2-hydoxy-2-methylpropiophenone (TCI, Shanghai Development Co., Ltd., Shanghai, China). Three mass ratios of PEGDMA and GelMA (2:1, 3:1, and 4:1, 1 represents 2% w/v here) were mixed in distilled water. 0.5% w/v photoinitiator was added to the prepolymer solution. The prepolymer solution was filled in a syringe without adaptor part and exposed to 365 nm UV light for crosslinking purposes. The exposure time was 15, 30, 45, and 60 s for each mass ratio of GelMA and PEGDMA. The crosslinked hydrogel within the syringe was 4 cm in length and then pressed through scientific sieves, at about 100 and 300 μm, respectively. PEGDMA pressed through sieves had become noodles and was collected in a water-filled petri dish and kept for further observation under a microscope for measurement of diameter of noodles.

Preparation of Magnetically Actuated Hydrogel Noodles: To fabricate a "magnetically actuated" layer of hydrogel noodles, a PEGDMA droplet (20% w/v, 200 μL) encapsulating one iron microsphere (200 μm diameter, nickel-coated) (K&J Magnetics) was added to the end of each hydrogel noodle, which subsequently underwent a photocrosslinking process. The other end of each hydrogel noodle was composed of a constrained layer fabricated using the same method, which was encapsulated with more microspheres (10–15) inside. All of the fabricated magnetically actuated hydrogel noodles were left to swell in DPBS for 24 h and then used for mechanical testing.

Uniaxial Stretching of Hydrogel Noodles: To apply uniaxial stretching to magnetic-actuated hydrogel noodles, two NdFeB magnets (22 mm × 5 mm × 2.5 mm, K&J Magnetics) fixed on a linear stage (Winner Optical instruments Group Co., Ltd., Beijing, China) were used. One permanent magnet was moved and applied to stretch the "magnetically actuated" layer of hydrogel noodles, and another one was utilized to fix the constrained layer.

Finite Element Simulation: To characterize the mechanical fields within hydrogel noodles, we performed a series of numerical simulations using commercially available software (COMSOL Multiphysics 4.0a, Comsol Inc.). Firstly, we predicted the magnetic field gradients experienced by the iron microspheres within the magnetically actuated layers as a function of the separation between the ends of the magnets and the centers of the iron microspheres. The magnetic force vector ($\vec{F}$) applied to each iron microsphere was estimated according to

$$\vec{F} = \int_A \mu_0^{-1} M_{sat} \bar{\nabla} \vec{B}(\vec{x}) \vec{n}(\vec{x}) d \tag{1}$$

where A is the surface of the iron microsphere, $\vec{n}$ is the outward normal of dA, μ_0 is the magnetic permeability of a vacuum, M_{sat} is the saturation moment of an individual iron microsphere, and $\bar{\nabla}\vec{B}(\vec{x})$ is the external magnetic field gradient tensor at position $\vec{x}$. This force was subsequently applied to a hydrogel noodle as a uniform pressure on the "magnetically actuated" layer; in-plane displacements were constrained to be zero on the constrained layer of hydrogel noodle, and all displacements were constrained to be zero on the constrained layer. These boundary conditions are appropriate given the difference in stiffness between the PEGDMA and PEGDMA/GelMA layers. PEGDMA/GelMA was treated as an incompressible, isotropic, Neo-Hookean material with elastic modulus derived from experimental work described below.

Mechanical Characterization of Hydrogel Noodles: To experimentally characterize magnetic force applied to iron microspheres in magnetically actuated layers, the Stokes drag method was used. An iron microsphere was placed in a poly(ethylene oxide) solution of defined viscosity (PEO; Sigma-Aldrich), then subjected to a magnetic field. The speed of each iron microsphere was estimated as a function of separation between the end of the magnetic field focuser and the center of the iron microsphere from video taken through a 20× objective, acquired using a high-speed camera (Phantom Cinestream v.711, Vision Research, Co., Ltd.) at 2500 images per second. The force exerted on the iron microsphere was then estimated using

$$F_{\text{magnetic}} = 6\pi R \nu \vec{U} + ma \tag{2}$$

Here the first term represents viscous drag, in which ν is the dynamic viscosity of the PEO solution, R is the radius of the iron microsphere, and U is the speed of the iron microsphere; and the second term represents an inertial force, in which m is the mass of the iron microsphere and a is the acceleration. The dynamic viscosity, ν, was estimated similarly from downward motion of iron microspheres released into a beaker of PEO solution in the absence of magnetic fields. The magnetic flux intensity was measured using a Teslameter (LZ-610H, Changsha 3D Measuring Equipment Co. Ltd.)

During stretching of hydrogel noodles, strain was estimated optically from images recorded using a high-resolution inverted fluorescent microscopy (IX-81, Olympus, Inc.) and analyzed using Image-Pro Plus (IPP; version 6.0, Media Cybernetics). Nominal strain, ε, was calculated in each layer as $\varepsilon = \lambda - 1$, with λ being the ratio of the current to initial length of the layer. The relationship between the Cauchy stress (force divided by current cross-sectional area) and this strain was found to be

linear over a very broad range of strains for all GelMA concentrations tested. The elastic moduli of the synthetic tissues were derived from these relationships.

Cell Encapsulation: C2C12 myoblasts were cultured in DMEM (Sigma-Aldrich) supplemented with 10% fetal bovine serum (GIBCO) in a 5% CO_2-humidified incubator at 37 °C. To collect and encapsulate cells, the cells were first trypsinized with 0.25% trypsin (Sigma-Aldrich) and centrifuged at 800 rpm for 5 min. The cells were suspended in 4% w/v PEGDMA and 2% w/v GelMA dissolved in DPBS at a density of 1×10^6 mL^{-1}, and then mixed with 0.5% w/v of photoinitiator. Cell-encapsulating hydrogel noodles were then photocrosslinked by exposing them to 365 nm UV light at a power of 2.9 mW cm^{-2} (model XLE-1000 A/F, Spectroline) for 45 s. The cell encapsulating noodles were then washed with DPBS three times and incubated. Culture medium is exchanged twice a day during culturing.

Structure Characterization of Microfluidic Hydrogels: For sample preparation, the hydrogel was placed into the freeze-drying chamber of a freeze-dryer (VFD-2000, Boyikang, Beijing, China) at −70 °C for 3 h. The frozen samples were subsequently dehydrated at −40 °C for 8 h, −25 °C for 5 h, 0 °C for 5 h, and 25 °C for 5 h. The freeze-dried specimens were submerged into liquid nitrogen for about 5 min and then fractured with a scalpel blade. The pore structure of hydrogel noodles was sputter coated with platinum (JFC-1600, JEOL), and the specimens were examined using a JEOL JSM-6700F SEM.

Cell Viability and Proliferation Characterization: To measure cell viability and proliferation, cells encapsulated in hydrogel noodles were stained with using a live/dead assay (Molecular Probes) following manufacturer's instructions. Briefly, each hydrogel noodle was incubated in a solution of 2 μg mL^{-1} calcein AM and 5 μg mL^{-1} propidium iodide at 37 °C for 30 min. Confocal microscopy (LSM 700, Carl Zeiss) was performed to identify cells that were living (stained green by calcein AM) and dead (stained red by propidium iodide). Live/dead cells and cell spread areas were both counted from these images using IPP. Briefly, one florescent image of noodle sample was imported in IPP software and was firstly split in different color channels (green was used here for cell area and number quantification). Here we used calcein-AM as a label to reveal cell morphology because it is hydrophobic and easy to penetrate the cell membrane with good dispersion in the cytoplasm. Then, the "Area" option in "count/size-measure-select measurement" menu was selected here. Finally, the cell area and number was calculated through "count/size-count" option. The cell distribution is uniform in both central and edge area of noodle sample (demonstrated by analysis of confocal images, as shown in Figure S11, Supporting Information). To avoid the effect of strong florescent signal along the noodle edges (caused by strong bias light and edge effect), we only analyzed central area of cells for each noodle sample.

Cell Orientation Analysis: To analyze the cell alignment, F-actin stress fibers and nuclei of cells were stained by fluorescein isothiocyanate (FITC) conjugated phalloidin (Acti-stain rhodamine phalloidin, Cytoskeleton, Inc.) and 4′, 6-diamidino-2-Phenylindole (DAPI; InvitrogenTM, Life Technologies, Inc.), respectively. Briefly, for stress fiber staining, cells in hydrogel noodles were fixed by 4% formaldehyde (Sigma-Aldrich) for 10 min, permeabilized with 0.5% Triton X-100 (Sigma-Aldrich) for 5 min, and then incubated with 200 μL of 100×10^{-9} M FITC phalloidin solution in the dark at room temperature for 30 min. For nuclear staining, cells were counterstained with 200 μL of 100×10^{-9} M DAPI in DPBS for 5 min. The images were analyzed to extract the orientation distribution and mean orientation of cells using the semi-automated "binarization-based extraction of alignment score" method described elsewhere.[59] Briefly, thresholded images were analyzed using a simple optimization scheme to identify the likelihood of cells possessing a dominant axis in directions ranging from 0° to 180°. The distributions were normalized.

Immunostaining of C2C12 Myotubes: C2C12 myotubes in hydrogel noodles were fixed by 4% formaldehyde for 20 min, followed by a wash with DPBS for three times. The permeabilization step was done with 0.5% Triton X-100 for 10 min at room temperature. Then, the cells were exposed to 5% bovine serum albumin dissolved in DPBS for 15 min. A primary mouse monoclonal IgG antibody (ab-7784, Abcam, Japan) against myosin heavy chain (MyHC) was added to the underlying sample at a dilution of 1:1000 in DPBS, and the samples were incubated at 4 °C overnight. The sample was then washed three times with DPBS, treated with a goat antimouse AlexaFluor 488 antibody (ab-150113, Abcam, Japan) at a dilution of 1:1000 in DPBS, and incubated at 37 °C for 1 h. The samples were then stained with nuclei according to the same protocol as mentioned before. The stained C2C12 myotubes were then imaged with confocal microscopy.

Western Blot Analysis: Cells or myotubes were isolated using RIPA lysis and extraction buffer with protease inhibitor (Beyotime). Protein concentration was determined using the BCA Protein Assay kit (Pierce of Thermo Scientific, Rockford, IL) according to manufacturer's protocols. Each protein sample was applied to SDS-PAGE gels, transferred to pure nitrocellulose membranes (PerkinElmer Life Sciences, Boston, MA, USA) and blocked with 5% nonfat milk. The membranes were incubated with the first antibody at 4 °C overnight. Then, the membranes were incubated with antirabbit or antimouse secondary antibodies at room temperature for 1 h. Chemiluminescent detection was performed using an ECL western blotting detection kit (Thermo Fisher, Rockford, IL, USA). Images were analyzed by Quantity One software (Bio-Rad, Shanghai, China).

Real-Time PCR: Total RNA was extracted from the cells and purified following the manufacturer's protocol (DNA/RNA Protein Isolation Kit (DP423). Reverse transcription was performed using the PrimeScript real-time PCR Kit (Takara, Dalian, China) followed by semi-quantitative real-time PCR using specific primers. The primer sequences were as follows: MyHC IId/x, 5′-GCGACAGACACCTCCTTCAAG-3′(forward) and 5′-TCCAGCCAGCCAGCGATG-3′ (reverse); Myod, 5′-CCAGGAC ACGACTGCTTTCT-3′ (forward) and 5′-TCTGGTGAGTCGAAACACGG-3′ (reverse); Myogenin, 5′-GAGACATGAGTGCCCTGACC-3′ (forward) and 5′-AGGCTTTGGAACCGGATAGC-3′ (reverse); Mrf4, 5′-CGAAAGG AGGAGACTAAAG-3′ (forward) and 5′-CTGTAGACGCTCAATGTAG-3′ (reverse). The expression of target genes was normalized against the GAPDH gene.[60] Real-time PCR was performed using the 7500 Fast Real-Time PCR System (Life Technologies, Inc.) with 0.8 μL of cDNA, 0.4 μL of the primer set, 3.8 μL of ddH_2O, and 5 μL of SYBR Green (Takara, Dalian, China). Following an initial denaturation step at 95 °C for 30 s, real-time PCR was performed over 45 cycles at 95 °C for 5 s, and 60 °C for 30 s, followed by a melting curve analysis. Gene expression analysis was repeated at least three times for each sample.

Statistical Analysis: All data collected were presented as the mean ± standard deviation (SD) of 10 samples. A Student's *t*-test was used to compare the data sets. A *p*-value of 0.05 or less was considered statistically significant.

Supporting Information

Supporting Information is available from the Wiley Online Library or from the author.

Acknowledgements

Y.L. and C.T.P. contributed equally to this work. Y.L., C.T.P., and F.X. conceived of the project. Y.L. and C.T.P. performed the experiments and collected the data. Y.L., C.T.P., B.P., and F.X. were involved in design and interpretation of the experiments. All authors participated in preparation of the manuscript. This work was financially supported by the National Natural Science Foundation of China (11372243), the Major International Joint Research Program of China (11120101002), and the International Science & Technology Cooperation Program of China (2013DFG02930). C.T.P. and B.P.-M. were also partially supported by the University of Malaya Research Grant RG320-14AFR and High Impact Research Grant UM-MOHE UM.C/HIR/MOHE/Eng/44 from the Ministry of Higher Education Malaysia. F.X. was also partially supported by the China Young 1000-Talent Program and Program for New Century Excellent Talents in

University (NCET-12-0437). Chinese Hele noodle fabrication (Intangible Cultural Heritage (ICH) of China) video was taken in Yong Xing Fang in Shaanxi province. This work was performed at the Bioinspired Engineering and Biomechanics Center (BEBC) at Xi'an Jiaotong University.

Received: May 15, 2015
Revised: July 7, 2015
Published online: August 12, 2015

[1] B. J. Vakoc, R. M. Lanning, J. A. Tyrrell, T. P. Padera, L. A. Bartlett, T. Stylianopoulos, L. L. Munn, G. J. Tearney, D. Fukumura, R. K. Jain, B. E. Bouma, *Nat. Med.* **2009**, *15*, 1219.
[2] V. J. Wedeen, D. L. Rosene, R. Wang, G. Dai, F. Mortazavi, P. Hagmann, J. H. Kaas, W. Y. Tseng, *Science* **2012**, *337*, 1605.
[3] S. Schiaffino, C. Reggiani, *Physiol. Rev.* **2011**, *91*, 1447.
[4] Y. Li, G. Huang, X. Zhang, L. Wang, Y. Du, T. J. Lu, F. Xu, *Biotechnol. Adv.* **2014**, *32*, 347.
[5] L. Madden, M. Juhas, W. E. Kraus, G. A. Truskey, N. Bursac, *Elife* **2015**, *4*, e04885.
[6] H. Onoe, T. Okitsu, A. Itou, M. Kato-Negishi, R. Gojo, D. Kiriya, K. Sato, S. Miura, S. Iwanaga, K. Kuribayashi-Shigetomi, Y. T. Matsunaga, Y. Shimoyama, S. Takeuchi, *Nat. Mater.* **2013**, *12*, 584.
[7] A. Badura, M. Schonewille, K. Voges, E. Galliano, N. Renier, Z. Gao, L. Witter, F. E. Hoebeek, A. Chedotal, C. I. De Zeeuw, *Neuron* **2013**, *78*, 700.
[8] Y. Jun, E. Kang, S. Chae, S. H. Lee, *Lab Chip* **2014**, *14*, 2145.
[9] M. Yamada, S. Sugaya, Y. Naganuma, M. Seki, *Soft Matter* **2012**, *8*, 3122.
[10] M. Hu, R. Deng, K. M. Schumacher, M. Kurisawa, H. Ye, K. Purnamawati, J. Y. Ying, *Biomaterials* **2010**, *31*, 863.
[11] Y. Liu, S. Sakai, M. Taya, *J. Biosci. Bioeng.* **2012**, *114*, 353.
[12] B. G. Chung, K. H. Lee, A. Khademhosseini, S. H. Lee, *Lab Chip* **2012**, *12*, 45.
[13] K. H. Lee, S. J. Shin, Y. Park, S. H. Lee, *Small* **2009**, *5*, 1264.
[14] E. Kang, G. S. Jeong, Y. Y. Choi, K. H. Lee, A. Khademhosseini, S. H. Lee, *Nat. Mater.* **2011**, *10*, 877.
[15] M. Akbari, A. Tamayol, V. Laforte, N. Annabi, A. H. Najafabadi, A. Khademhosseini, D. Juncker, *Adv. Funct. Mater.* **2014**, *24*, 4060.
[16] S. Arumuganathar, S. N. Jayasinghe, *Biomacromolecules* **2008**, *9*, 759.
[17] D. Puppi, D. Dinucci, C. Bartoli, C. Mota, C. Migone, F. Dini, G. Barsotti, F. Carlucci, F. Chiellini, *J. Bioact. Compat. Pol.* **2011**, *26*, 478.
[18] M. F. Leong, J. K. Toh, C. Du, K. Narayanan, H. F. Lu, T. C. Lim, A. C. Wan, J. Y. Ying, *Nat. Commun.* **2013**, *4*, 2353.
[19] L. G. Griffith, G. Naughton, *Science* **2002**, *295*, 1009.
[20] D. Seliktar, R. M. Nerem, Z. S. Galis, *Tissue Eng.* **2003**, *9*, 657.
[21] G. Giavaresi, P. Torricelli, P. M. Fornasari, R. Giardino, R. Barbucci, G. Leone, *Biomaterials* **2005**, *26*, 3001.
[22] N. L'Heureux, N. Dusserre, G. Konig, B. Victor, P. Keire, T. N. Wight, N. A. Chronos, A. E. Kyles, C. R. Gregory, G. Hoyt, R. C. Robbins, T. N. McAllister, *Nat. Med.* **2006**, *12*, 361.
[23] D. Seliktar, R. A. Black, R. P. Vito, R. M. Nerem, *Ann. Biomed. Eng.* **2000**, *28*, 351.
[24] S. Sugiura, T. Oda, Y. Aoyagi, M. Satake, N. Ohkohchi, M. Nakajima, *Lab Chip* **2008**, *8*, 1255.
[25] N. A. Raof, M. R. Padgen, A. R. Gracias, M. Bergkvist, Y. B. Xie, *Biomaterials* **2011**, *32*, 4498.
[26] S. Zhang, M. A. Greenfield, A. Mata, L. C. Palmer, R. Bitton, J. R. Mantei, C. Aparicio, M. O. de la Cruz, S. I. Stupp, *Nat. Mater.* **2010**, *9*, 594.
[27] X. Shi, S. Ostrovidov, Y. Zhao, X. Liang, M. Kasuya, K. Kurihara, K. Nakajima, H. Bae, H. Wu, A. Khademhosseini, *Adv. Funct. Mater.* **2015**, *25*, 2250.
[28] B. K. Mann, A. T. Tsai, T. Scott-Burden, J. L. West, *Biomaterials* **1999**, *20*, 2281.
[29] B. K. Mann, R. H. Schmedlen, J. L. West, *Biomaterials* **2001**, *22*, 439.
[30] P. McMillen, S. A. Holley, *Curr. Opin. Genet. Dev.* **2015**, *32*, 106.
[31] J. K. Mouw, Y. Yui, L. Damiano, R. O. Bainer, J. N. Lakins, I. Acerbi, G. Ou, A. C. Wijekoon, K. R. Levental, P. M. Gilbert, E. S. Hwang, Y. Y. Chen, V. M. Weaver, *Nat. Med.* **2014**, *20*, 360.
[32] J. Huegel, A. A. Williams, L. J. Soslowsky, *Curr. Rheumatol. Rep.* **2015**, *17*, 476.
[33] M. P. Lutolf, J. A. Hubbell, *Nat. Biotechnol.* **2005**, *23*, 47.
[34] J. P. Medema, L. Vermeulen, *Nature* **2011**, *474*, 318.
[35] J. L. Tan, J. Tien, D. M. Pirone, D. S. Gray, K. Bhadriraju, C. S. Chen, *Proc. Natl. Acad. Sci. USA* **2003**, *100*, 1484.
[36] R. Kaunas, S. Usami, S. Chien, *Cell Signal.* **2006**, *18*, 1924.
[37] X. Trepat, M. R. Wasserman, T. E. Angelini, E. Millet, D. A. Weitz, J. P. Butler, J. J. Fredberg, *Nat. Phys.* **2009**, *5*, 426.
[38] J. Lee, A. A. Abdeen, D. Zhang, K. A. Kilian, *Biomaterials* **2013**, *34*, 8140.
[39] M. Ghibaudo, J. M. Di Meglio, P. Hersen, B. Ladoux, *Lab Chip* **2011**, *11*, 805.
[40] E. Cukierman, R. Pankov, D. R. Stevens, K. M. Yamada, *Science* **2001**, *294*, 1708.
[41] T. Wakatsuki, M. S. Kolodney, G. I. Zahalak, E. L. Elson, *Biophys. J.* **2000**, *79*, 2353.
[42] J. Foolen, V. S. Deshpande, F. M. Kanters, F. P. Baaijens, *Biomaterials* **2012**, *33*, 7508.
[43] J. W. Nichol, S. T. Koshy, H. Bae, C. M. Hwang, S. Yamanlar, A. Khademhosseini, *Biomaterials* **2010**, *31*, 5536.
[44] F. Xu, F. Inci, O. Mullick, U. A. Gurkan, Y. Sung, D. Kavaz, B. Li, E. B. Denkbas, U. Demirci, *ACS Nano* **2012**, *6*, 6640.
[45] G. Y. Huang, X. H. Zhang, Z. P. Xiao, Q. C. Zhang, J. X. Zhou, F. Xu, T. J. Lu, *Soft Matter* **2012**, *8*, 10687.
[46] U. A. Gurkan, Y. Fan, F. Xu, B. Erkmen, E. S. Urkac, G. Parlakgul, J. Bernstein, W. Xing, E. S. Boyden, U. Demirci, *Adv. Mater.* **2013**, *25*, 1192.
[47] Y. Fan, F. Xu, G. Huang, T. J. Lu, W. Xing, *Lab Chip* **2012**, *12*, 4724.
[48] A. Nakayama, A. Kakugo, J. P. Gong, Y. Osada, M. Takai, T. Erata, S. Kawano, *Adv. Funct. Mater.* **2004**, *14*, 1124.
[49] P. Tseng, J. W. Judy, D. Di Carlo, *Nat. Methods* **2012**, *9*, 1113.
[50] W. R. Legant, J. S. Miller, B. L. Blakely, D. M. Cohen, G. M. Genin, C. S. Chen, *Nat. Methods* **2010**, *7*, 969.
[51] M. S. Hall, R. Long, C. Y. Hui, M. M. Wu, *Biophys. J.* **2012**, *102*, 2241.
[52] K. Shimizu, H. Fujita, E. Nagamori, *Biotechnol. Bioeng.* **2009**, *103*, 631.
[53] S. A. Riboldi, M. Sampaolesi, P. Neuenschwander, G. Cossu, S. Mantero, *Biomaterials* **2005**, *26*, 4606.
[54] E. D. Ker, A. S. Nain, L. E. Weiss, J. Wang, J. Suhan, C. H. Amon, P. G. Campbell, *Biomaterials* **2011**, *32*, 8097.
[55] J. Ramon-Azcon, S. Ahadian, M. Estili, X. B. Liang, S. Ostrovidov, H. Kaji, H. Shiku, M. Ramalingam, K. Nakajima, Y. Sakka, A. Khademhosseini, T. Matsue, *Adv. Mater.* **2013**, *25*, 4028.
[56] X. Wang, H. Li, A. Zheng, L. Yang, J. Liu, C. Chen, Y. Tang, X. Zou, Y. Li, J. Long, J. Liu, Y. Zhang, Z. Feng, *Cell Death Dis.* **2014**, *5*, 1521.
[57] S. Ahadian, J. Ramon-Azcon, M. Estili, X. Liang, S. Ostrovidov, H. Shiku, M. Ramalingam, K. Nakajima, Y. Sakka, H. Bae, T. Matsue, A. Khademhosseini, *Sci. Rep.* **2014**, *4*, 4271.
[58] D. H. Kim, J. Park, K. Y. Suh, P. Kim, S. K. Choi, S. Ryu, S. Park, S. H. Lee, B. Kim, *Sens. Actuators B: Chem.* **2006**, *117*, 391.
[59] F. Xu, T. Beyazoglu, E. Hefner, U. A. Gurkan, U. Demirci, *Tissue Eng. Part C: Methods* **2011**, *17*, 641.
[60] T. D. Schmittgen, K. J. Livak, *Nat. Protoc.* **2008**, *3*, 1101.